Probing the efficiency of thermal and photochemical bond homolysis in functionalized nanostructured SBA-15 silicas

Pierre Nabokoff, Stéphane Gastaldi, Eric Besson

Probing the efficiency of thermal and photochemical bond homolysis in functionalized nanostructured SBA-15 silicas

Pierre Nabokoff,[a] Stéphane Gastaldi,*[a] Eric Besson*[a]

[a] Aix Marseille Univ, CNRS, ICR, Marseille, France.

E-mail : stephane.gastaldi@univ-amu.fr, eric.besson@univ-amu.fr.

Highlights:

- Synthesis of thermally and/or photo-chemically activable alkoxyamine anchored SBA-15.
- Evidences for a homolysis reaction as efficient on silica than in solution, whatever the thermal or photochemical conditions.
- First determination of dissociation constants of alkoxyamines in functionalized mesoporous silicas.
- First proof for photochemical TEMPO-H bond homolysis.

Abstract: The formation of radical species in solution can be triggered through thermal or photochemical activation of a suitable precursor. This EPR study aimed to establish if these two activation modes were as effective in mesoporous silicas as in solution. First, a calibration system was devised and validated to reliably quantify the radical formation. Alkoxyamines were selected to generate stable nitroxyl radicals upon heating or irradiation. Thanks to direct synthesis by the sol-gel process, these precursors were selectively located on the pore surface or in the framework of mesoporous silicas. The thermal or photo-chemical activation of the functionalized materials showed that nitroxides were formed in yields comparable to those observed in solution. No significant differences were observed with the

implementation of these activation modes between the solution and the mesoporous silicas. Moreover, the thermal experiments enabled to measure the C-O bond dissociation constants of alkoxyamines covalently anchored to a nanostructured silica, their values were in the same order of magnitude than those determined in solution.

Graphical abstract:

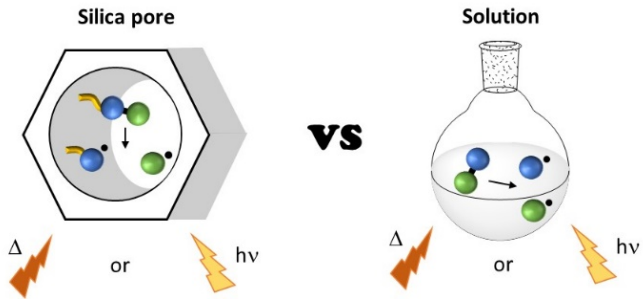

Keywords:

Hybrid mesoporous silica, EPR spectroscopy, Alkoxyamine, Homolysis kinetics, thermal and photochemical fragmentation

1. Introduction

Currently, the development of spin science relies on the use of stable or highly persistent radicals [1] which gather only a small part of paramagnetic organic species since most of them are transient. In order to increase the diversity of available radicals, strategies have been implemented to improve the persistence of transient radicals [2]. They aim to impede bimolecular reactions by limiting the diffusion of radicals or by inserting an external crowding. Confinement proved to be an efficient tool to make stable or persistent transient radicals. For this purpose, sophisticated tailor-made materials have been designed, they can roughly be split into two groups. In the first one, the radical precursors are inserted in highly ordered self-assembled systems such as MOF [3], COF [4], PMOS [5] or layered materials [6,7]. In the other group, the

paramagnetic species associate through non-bonding interactions to afford a wide array of systems capable to provide confinement. Porous materials (zeolite [8,9], AlMCM-41 [10]) and cage molecules (cucurbit[n]urils [11,12,13,14], cyclophanes [15], cyclodextrins [16], single-wall carbon nanotubes [17,18]) can be found in this latter group.

In this context, we developed another approach where the radical precursors were covalently linked to a mesoporous silica which provided confinement effect. The flexibility of the sol-gel process enabled the design of a wide range of structures in which the organic precursors were located either on the pore surface or in the framework of the silica. Upon irradiation or heating, the decomposition of diazene-based precursors led cleanly to the generation of the targeted radicals. These nanostructured systems enabled to considerably increase the lifetime of transient radicals such as phenoxyl [5,6], arylsulfanyl [6,19,20,21] or arylsulfinyl [22] radicals from hundreds of microseconds to hours, days and even years. The main difficulty encountered with these materials lied in the yields of generated radicals. Indeed, whatever the system under investigation, it ranged from 1 to 5%, which is much lower than expected. For the purpose of understanding these results, we decided to investigate the impact of the silica structure on the efficiency of radical generation triggered by photolysis or by thermolysis. From a general point of view, the EPR quantification of the amount of transient radicals generated all along a reaction is a tricky task since the signal registered is only representative of the radicals that are effectively present in the medium. It does not allow to evaluate how many radicals have evolved through termination. Namely, the EPR signal enables to determine the quantity of present radicals but not the quantity of generated radicals all along an experiment, and this is especially true with transient radicals.

It is the reason why this study was performed with a stable nitroxyl radical in order to evaluate exclusively the efficiency of the initiation method by suppressing any interferences relative to the elusive character of the generated radical. This approach enables a reliable quantification of the generated radicals since once formed the selected nitroxides do not evolve and their amount can be determined by means of a simple calibration curve. The goal of this work was to find out if the initiation methods were as effective in functionalized nanostructured silicas as in solution. To this end, the efficacy of homolytic cleavage was comparatively evaluated in three systems: (i) in solution as reference, (ii) with the radical precursors located on the pore surface and (iii) with the radical precursors located inside the wall of the silicas.

2. Experimental

All the procedures for the preparation of organic precursors and the corresponding functionalized silicas are detailed in supplementary data as well as their full characterizations. The syntheses of **3** and **SBA_n-3** are given as an example.

*2.1 Syntheses of alkoxysilane **11***

1-(Benzyloxy)-2,2,6,6-tetramethylpiperidin-4-ol (9): A solution of (bromomethyl)benzene (0.5 g, 2.9 mmol, 1 equiv), 4-hydroxy- TEMPO (0.5 g, 2.9 mmol, 1 equiv), 2,2'-bypridine (0.9 g, 5.8 mmol, 2 equiv), in acetonitrile (5 mL) was degassed 10 min by bubbling with argon. Then copper (0.19 g, 2.9 mmol, 1 equiv) was added and the mixture stirred overnight at room temperature. After addition of AcOEt (50 mL) the mixture was filtrated on a celite pad and the organic phase washed with a solution of $CuSO_4$ (5%), water (3 times) and brine. After drying over $MgSO_4$, the solution was evaporated to give 9 (0.65g, 2.47mmol, 85%). ^{1}H NMR (300 MHz, $CDCl_3$): 7.39 – 7.27 (m, 5H, Ar*H*), 4.83 (s, 2H, C*H*$_2$-O), 3.99 (td, J = 11.2, 4.8, 1H, C*H*-OH), 1.84 (dd, J = 12.4, 4.1, 2H, C*H*$_2$), 1.52 (t, J = 11.7, 7.7, 2H, C*H*$_2$), 1.30 (s, 6H, C*H*$_3$), 1.21 (s, 6H, C*H*$_3$).^{13}C NMR, (75 MHz, $CDCl_3$) δ: 138.1 (C_{Ar}), 128.4 (CH_{Ar}), 127.6

(CH_{Ar}), 127.6 (CH_{Ar}), 79.0 (CH_2-O), 63.5 (*C*H-OH), 60.5 (*C*-CH_3), 48.6 (CH_2), 33.4 (CH_3), 21.4 (CH_3). HRMS (ESI): m/z calculated for $[M+H]^+$ $C_{16}H_{26}NO_2^+$: 264.1885 Da, found 264.1953 Da.

4-(Allyloxy)-1-(benzyloxy)-2,2,6,6-tetramethylpiperidine (11): To a 0°C solution of **9** (1 g, 3.8 mmol, 1 equiv) in dry DMF (15 mL) was added NaH (0.18 g, 7.6 mmol, 2 equiv). The suspension was stirred 10 min at 0°C and then allylbromide (0.88 g, 7.6 mmol, 2 equiv) was slowly added. The resulting mixture was stirred overnight. The reaction was monitored by TLC. After completion, the mixture was diluted with water, and extracted three times with AcOEt. Organic extracts were washed with water and brine, dried over $MgSO_4$ and concentrated. The residue was purified using silica gel column (2/98 Et_2O/pentane to give **11** (1.1 g, 3.6 mmol, 95%).^{1}H NMR (300 MHz, $CDCl_3$) δ: 7.38 – 7.27 (m, 5H, Ar*H*), 6.02 – 5.84 (ddt, J = 17.2, 10.4, 5.6, 1H, C*H*=), 5.31 – 5.25 (dd, J = 17.2, 1.7, 2H, CH_2=), 5.18 – 5.14 (dd, J = 10.4, 1.3, 2H, CH_2=), 4.83 (s, 2H, CH_2-O), 4.00 (d, J = 5.6, 2H, CH_2-CH=), 3.63 (tt, J = 11.2, 4.1, 1H, C*H*-O), 1.88 (dd, J = 11.7, 3.0, 2H, CH_2), 1.54-1.45 (m, 2H, CH_2), 1.30 (s, 6H, CH_3), 1.20 (s, 6H, CH_3).^{13}C NMR, (75 MHz, $CDCl_3$) δ: 138.3 (C_{Ar}), 135.5 (*C*H=), 128.4 (CH_{Ar}), 127.6 (CH_{Ar}), 127.5 (CH_{Ar}), 116.7 (CH_2=), 79.0 (CH_2-O), 70.1 (*C*H-O), 69.3 (CH_2-O), 60.4 (*C*-CH_3), 45.3 (CH_2), 33.5 (CH_3), 21.40 (CH_3). HRMS (ESI): m/z calculated for $[M+H]^+$ $C_{19}H_{30}NO_2^+$: 304.2198 Da, found 304.2271 Da.

1-(benzyloxy)-2,2,6,6-tetramethyl-4-(2-(triethoxysilyl)ethoxy)piperidine (3): To compound **11** (1.1 g, 3.6 mmol, 1 equiv) under argon was added triethoxysilane (1.2 g, 7.2 mmol, 2 equiv) and Karstedt catalyst. The solution was stirred at room temperature overnight. The reaction was monitored by ^{1}H NMR. After completion, the mixture was concentrated, pentane was added, and the resulting solution filtrated under argon and concentrated. The product (**3**) was used without further purification (0.99 g, 2.2 mmol, 65%). ^{1}H NMR (300 MHz, $CDCl_3$): 7.35 – 7.29 (m, 5H, Ar*H*), 4.83 (s, 2H, CH_2-O), 3.83 (q, J=7.0, 6H, CH_2-O-Si),

3.56 (tt, J = 11.1, 4.1, 1H), 3.42 (t, J = 6.8, 2H, C*H*$_2$-O), 1.96-1.80 (m, 2H, C*H*$_2$), 1.75-1.63 (m, 2H, C*H*$_2$), 1.51-1.44 (m, 2H, C*H*$_2$), 1.32 – 1.19 (m, 21H, *CH*$_3$), 0.70 – 0.62 (m, 1H, C*H*$_2$-Si).^{13}C NMR, (75 MHz, $CDCl_3$): 138.3 (*C*$_{Ar}$), 128.3 (*C*H$_{Ar}$), 127.6 (*C*H$_{Ar}$), 127.5 (*C*H$_{Ar}$), 79.0 (*C*H_2-O-N), 70.5 (*C*H_2-O), 70.3 (CH-O), 60.4 (*C*-CH_3), 58.5 (*C*H_2-O-Si), 45.4 (*C*H_2) 33.4 (*C*H_3),23.6 (*C*H_2), 21.4 (*C*H_3), 18.4 (*C*H_3-CH_2-OSi), 6.7 (*C*H_2-Si). HRMS (ESI): m/z calculated for $[M+H]^+$ $C_{25}H_{46}NO_5Si^+$: 468.3067 Da, found 468.3141 Da.

2.2 Synthesis of SBA$_n$-3 silicas

SBA$_{28}$-3: In a typical procedure, pluronic P-123 (1 g) in deionized water (7 mL) and 2 M hydrochloric acid solution (30 mL) was stirred for 3h at 40 °C. tetraethoxysilane (4.03 g, 19.38 mmol, 38 equiv) and organic precursor **3** (0.480 g, 1.02 mmol, 1 equiv) were added. The mixture was stirred 24 h at 40 °C, then warmed without stirring at 100 °C for 2 days, filtrated, washed three times with water, twice with ethanol and acetone and finally extracted with a Soxhlet apparatus (ethanol) for 24h. The wet powder was filtrated, washed twice with acetone and diethylether. After one night at 80 °C under vacuum, a white powder was recovered. The molar composition of the synthesis mixture was as follows: (1-x) M TEOS: x M **3**: 0.017 M P123 Polymer: 188 M H_2O: 5.8 M HCl, where x denotes the number of moles of precursor **3**. ^{13}C CPMAS NMR (101.6 MHz) δ: 138.0, 127.9, 78.9, 71.9, 66.3, 61.2, 44.7, 40.3, 39.3, 32.2, 29.9, 20.8, 16.6, 8.1. ^{29}Si CPMAS NMR (79.5 MHz) δ: -64.4 (T^3), -91.8 (Q^2), -100.6 (Q^3), -109.7 (Q^4). BET Surface Area: 527 m²/g. BJH Desorption Average Pore Diameter: 6.8 nm. TGA: Mass Loss = 3.07%. SAXS: d = 10,67 nm, a = 12.31 nm.

SBA$_{108}$-3: Following the previous procedure, tetraethoxysilane (8,4 g, 40 mmol, 52 equiv) and organic precursor **3** (0.351 g, 0.77 mmol, 1 equiv). ^{13}C CPMAS NMR (101.6 MHz) δ: 137.9, 127.9, 79.1, 70.6, 66.3, 61.1, 59.3, 58.3, 44.6, 32.1, 29.7, 20.0, 16.4, 7.7. ^{29}Si CPMAS NMR (79.5 MHz) δ: -63.9 (T^3), -91.5 (Q^2), -100.6 (Q^3), -109.5 (Q^4). BET Surface Area: 835

m^2/g. BJH Desorption Average Pore Diameter: 6.5 nm. TGA: Mass Loss = 1,43%. SAXS: d = 10.79 nm, a = 12.38 nm

SBA_{227}-3: Following the previous procedure, tetraethoxysilane (8.4 g, 40 mmol, 95 equiv) and organic precursor 3 (191 mg, 0.42 mmol, 1 equiv). ^{13}C CPMAS NMR (101.6 MHz) δ: 127.9, 70.9, 66.6, 59.2, 44.5, 30,6, 19.6, 15.7, 8.1. ^{29}Si CPMAS NMR (79.5 MHz) δ: -63.4 (T^3), -91.3 (Q^2), -100.6 (Q^3), -109.6 (Q^4). BET Surface Area: 457 m^2/g. BJH Desorption Average Pore Diameter: 6.2 nm. TGA: Mass Loss = 4.1%. SAXS: d = 10.79 nm, a = 12.46 nm.

2.3 General procedure for irradiation of functionalized silica

2.3.1 Silica in suspension in terbutylbenzene

10 mg of functionalized silica were placed in a 4 mm quartz-glass tube and 300 µL of *tert*-butylbenzene were added. Silica was completely impregnated by agitation of the tube during 10 min. Irradiation at room temperature was directly performed within the EPR cavity until a maximum value of the double integrated signal was observed.

2.3.2 Experiments without solvent

10 mg of functionalized silica was placed in a 4 mm quartz-glass tube. Irradiation at room temperature was realized directly within the EPR cavity until a maximum value of the double integrated signal was observed.

2.3.3 Experiments with different solvents

100 mg of functionalized silica in 3 mL of the appropriate solvent were placed in a quartz tube and irradiated at 365 nm at room temperature during 3h. The suspension was then filtered, the silica was washed twice with ethanol, twice with acetone, once with Et_2O and

then dried under *vacuo* at 60°C overnight. Subsequently 10 mg of the irradiated silica were placed in a 4 mm quartz-glass tube and analyzed *via* EPR.

2.4 General procedure for thermal activation of functionalized silica

10 mg of functionalized silica were placed in a 4 mm quartz glass tube and 300 µL of *tert*-butylbenzene were added. Silica was completely impregnated by agitation of the tube during 10 min. The sample was then placed within the EPR resonator, the recording of the signal started at room temperature, then the resonator was heated at 130°C. The signal was recorded from 2 hours to overnight. The sample was then cooled down to room temperature, the double integrated signal was recorded. If the maximum intensity of the signal was not reached, the sample was heated again at 130°C using an oil bath. The decomposition of the alcoxyamines was regularly monitored by EPR at room temperature until no increase of signal intensity was observed.

3. Results and discussion

3.1 Design and syntheses of alkoxysilane precursors

The two model molecules **1** and **2** were selected to evaluate the efficiency of thermal or photo-chemical cleavage methods (Figure 1), both precursors lead to the formation of a nitroxyl radical, i.e. the TEMPO.

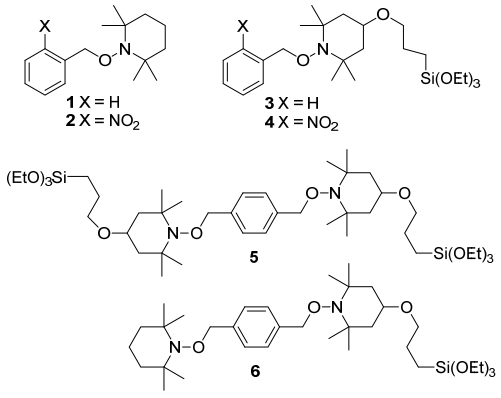

Figure 1. Alkoxyamine structures

Upon heating, the C-O bond homolysis of benzylic alkoxyamine **1** reversibly leads to the direct formation of a stable TEMPO and a benzylic radical which is either trapped by dioxygen or dimerizes (Scheme 1). The presence of a radical trap, such as dioxygen, is crucial to increase the alkoxyamine decay rate [23]. The *ortho*-nitro benzylic alkoxyamine **2** was chosen to assess the photochemical process [24]. The irradiation of **2** induces the formation of TEMPO following the mechanism described in Scheme 2 [25,26]. In this case, TEMPO is formed in a subsequent oxidation step [27].

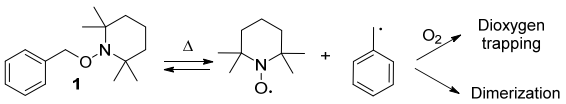

Scheme 1. Thermal homolysis mechanism of **1**

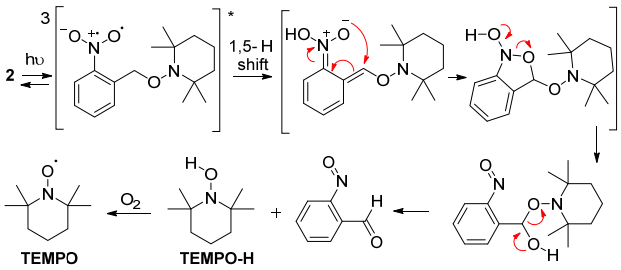

Scheme 2. Fragmentation mechanism of **2**

With these two reactions, the effectiveness of the initiation methods can be correlated to the yield of formation of TEMPO. **1** and **2** were used to benchmark the initiation methods in solution. The heating or the irradiation can be achieved in the cavity of an EPR spectrometer and the yield directly calculated thanks to a reference solution. Analog probes were designed to prepare radical precursors covalently bonded to SBA-15 mesoporous silicas. The functionalized mesoporous silicas incorporating **3** and **4** were used to perform the very same reactions in the pores whereas the material derived from **5** aimed at studying the thermal homolysis leading to nitroxides located in the framework of the silicas. In this case, the homolysis lead to two face-to-face nitroxides embedded in the silica walls. In order to

compare the impact of the surroundings, pore or wall, on the thermal homolysis reaction, bis-alkoxyamine **6** was designed with a structure as similar as possible to that of **5**.

3.2 Material syntheses

All the precursors were straightforwardly prepared from the corresponding benzylbromides (Scheme 3) in 1 or 3 steps: (i) trapping of the benzylic radicals with TEMPO or TEMPOL, (ii) formation of an allyl ether and (iii) hydrosilylation to introduce the trialkoxysilane group necessary for the preparation of the hybrid materials.

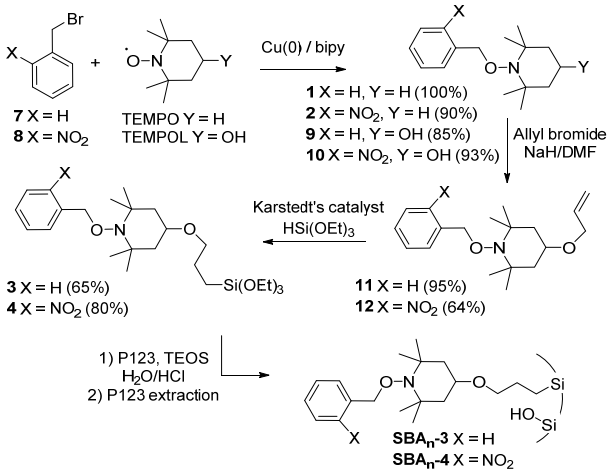

Scheme 3. Synthesis of alkoxyamine precursors **1** and **2**, and silicas **SBA$_n$-3** and **SBA$_n$-4**

The synthesis of mesoporous silicas via the sol-gel process in the presence of structure-directing agents (P123 ($PEO_{20}PPO_{70}PEO_{20}$)) and tetraethoxysilane (TEOS) led to functionalized organic-inorganic hybrid nanostructured materials in which the organic moiety is specifically localized either on the pore surface or inside the framework of the silica pores [28,29]. Indeed, the number of trialkoxysilane groups in the organic precursor determines its location in the silica. The presence of a single silylated group enables the location of the organic moiety on the pore surface (Scheme 3) whereas an additional trialkoxysilane function positions the organic linkage in the framework, thanks to the

hydrophilicity of the two trihydroxysilyl groups generated at each end under the acidic conditions of the sol-gel process. The preparation of **SBA$_{56}$-5** had already been reported (Scheme 4) [30].

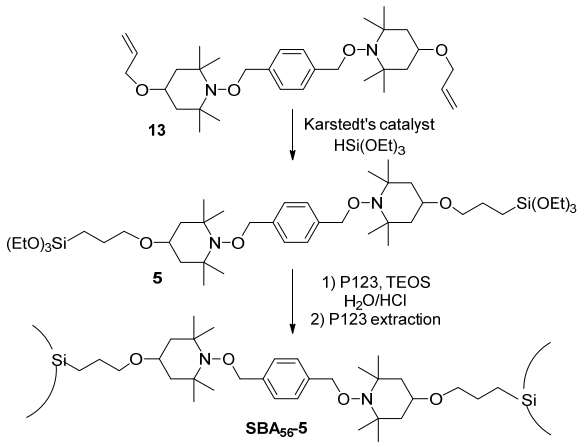

Scheme 4. Synthesis of wall-functionalized nanostructured silicas **SBA$_{56}$-5**[30]

The synthesis of bis-alkoxyamine **14** was based on a statistical desymmetrisation of α,α′-dibromo-*p*-xylene thanks to the trapping of the benzylic radical with an equimolar mixture of TEMPO and TEMPOL (Scheme 5). The conversion of **14** into **SBA$_{92}$-6** involved transformations identical to previously described ones.

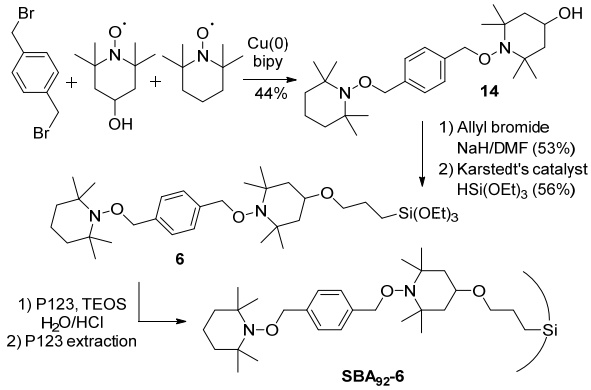

Scheme 5. Synthesis of pore-functionalized nanostructured silicas **SBA$_{92}$-6**

The resulting materials were named **SBA$_n$-3**, **SBA$_n$-4**, **SBA$_{56}$-5** and **SBA$_{92}$-6** in which **3**, **4**, **5** and **6** specify the nature of the organic precursor and n indicates the TEOS/radical precursor molar ratio determined after the characterization of the hybrid silicas. It is

worth noting that an increase of the n value corresponds to an increased dilution of the radical precursor in the materials. Three different loadings were prepared for **SBA_n-3** (n=28, 108, 227) and **SBA_n-4** (n=52, 78, 283) (See supplementary data). So as to investigate the effect of the surface silanols on the nitroxide formation, silicas **SBA_n-3***, **SBA_n-4*** and **SBA_{92}-6*** were prepared by passivation of **SBA_n-3**, **SBA_n-4** and **SBA_{92}-6** with $ClSiMe_3$ in toluene. The substitution of the silanol hydroxyl groups by hydrophobic trimethylsilyl groups suppresses the surface hydrogen bonds. All these materials were fully characterized by standard procedures (NMR, SAXS, nitrogen adsorption / desorption analysis, thermogravimetric analysis (TGA) (see supplementary data)).

3.3 Calibration systems

EPR spectrometry was used to measure the quantity of generated radicals. For the solution experiments, the quantification of TEMPO was classically performed with a 10^{-4} M reference solution of TEMPO in *tert*-butylbenzene. It was not possible to use the same method in the case of TEMPO covalently linked to the silica. Indeed, the shape and the intensity of the EPR signal depend on the 3D structure of the silica and the radical distribution as evidenced in the design of TEMPO functionalized silicas for DNP NMR applications [31]. This is the reason why two approaches were investigated to set up a reliable calibration system. In the first one, TEMPO was simply adsorbed on a mesoporous silica at different concentrations. It must be underlined that in order to avoid any bias related to the loss of TEMPO by sublimation during the preparation of these silicas, the concentration of adsorbed TEMPO was corroborated by TGA. In the second one, a series of three TEMPO functionalized silicas were prepared according to the same direct synthesis method, so that their features were as similar as possible to the materials of interest for this study in term of both homogeneity of distribution of the organic moieties and 3D structure (Scheme 6). As previously mentioned, **SBA_n-16**

materials were fully characterized by standard methods and the loading, i.e. the TEMPO concentration, was determined by TGA.

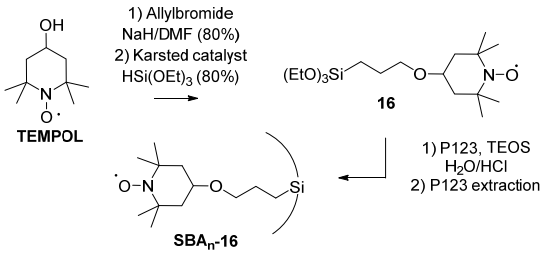

Scheme 6. Synthesis of TEMPO functionalized silicas **SBA$_n$-16**

All these reference samples were analysed by EPR and the calibration lines were drawn from the double integrated EPR signal and the concentration in nitroxide (Figure 2). It must be underlined that in the case of **SBA$_n$-16**, the presence or the absence of *tert*-butylbenzene did not change the calibration line. A simple comparison between these lines showed significant differences between these three systems.

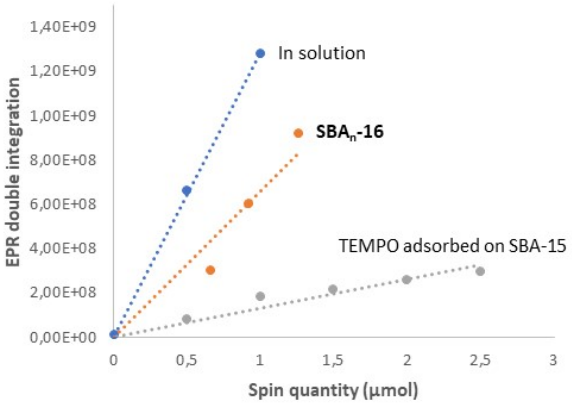

Figure 2. Calibration lines for TEMPO in solution in *tert*-butylbenzene (blue line), adsorbed on SBA-15 (grey line) and covalently linked to **SBA$_n$-16** (orange line).

As suspected, the close surrounding of the nitroxide had a strong impact on the EPR signal as well as on its shape as on its intensity. Indeed, the surface signal was roughly four times higher for **SBA$_n$-16** than for adsorbed references, it was even larger for the TEMPO solution. This might be explained by a difference in the nitroxide distribution in the EPR sample. As a

matter of fact, for a given radical concentration, the signal intensity increased from nitroxide adsorbed on the pore surface, for which there is a well-known non-homogeneous distribution on the pore surface, to **SBA$_n$-16**, in which there is a homogenous distribution on the pore surface thanks to the sol-gel process by direct synthesis, and finally the TEMPO solution which has a homogenous volumetric distribution. So as to validate one of these calibration systems, a suspension of **SBA$_{108}$-3** was heated in a EPR cavity at 130 °C until the signal reached a quasi-stationary state. After 48 h all the C-O bonds were cleaved, a TGA was performed on this sample. Considering the loading of **SBA$_{108}$-3** before heating, the loss of mass confirmed the total fragmentation of the alkoxyamine moieties and enabled to determine the concentration in TEMPO which fitted the second calibration system with the covalently linked nitroxide. Accordingly, **SBA$_n$-16** materials were used as reference for all the measures performed in this study.

3.4 Thermal homolysis

The homolysis of **1** is known to proceed at a temperature close to 130 °C [23]. Concerning **SBA$_n$-3** materials, the temperature of homolytic cleavage was determined by means of TGA on **SBA$_{28}$-3**. It is consistent with the value in solution. Indeed, the fragmentation of **SBA$_n$-3** occurred between 130 and 240 °C, the formation of a benzylic radical was evidenced by mass spectroscopy coupled TGA (Figure 3). It must be underlined that this specific loss of weight, i.e. a benzylic moiety, was used as fingerprint to efficiently quantify the alkoxyamine loadings of the functionalized silicas.

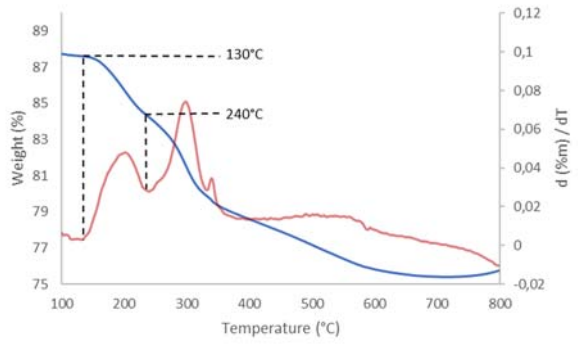

Figure 3. Thermogravimetric analysis of **SBA_{28}-3**

A 10^{-4}M solution of alkoxyamines **1** and **2** were directly heated at 130 °C in *tert*-butylbenzene in the EPR cavity. After 15 h, the signal reached a quasi-stationary state and, thanks to the calibration line, yields about 90% were determined (Table 1). These values were used as benchmark for this study. Similarly, a suspension of **SBA_n-3**, **SBA_n-3*** and **SBA_n-4** in EPR tubes were heated in an oil bath at the same temperature. The heating times needed to reach a stationary state, i.e. a stop in the EPR signal growth, ranged between 59 and 102 h. Very good yields, higher than 91%, were measured for the materials except for **SBA_{283}-4** for which a slight decrease of yield (67%) was recorded, a phenomenon for which we found no obvious explanation. Moreover, **SBA_n-3*** showed that the passivation had no effect on the efficacy of the homolysis as well on the yield as the reaction time. The same experiment was performed at a slightly higher temperature, 160 °C, on **SBA_{108}-3**. Under these conditions a maximum yield of 82% was reached after 15 h, then a slow decomposition of the nitroxide occurred. It remained only 31% of radicals after 80 h at 160 °C whereas no degradation was registered after the same period at 130 °C.

Table 1. k_d, E_a, $t_{1/2}$ and thermal homolysis yields at 130 °C of **1**, **2**, **SBA_n-3**, **SBA_n-3***, **SBA_n-4**, and **SBA_{56}-5**, **SBA_{92}-6** and **SBA_{92}-6***.

	$t_{1/2}$ (h)	Yield (%)	E_a (kJ/mol)	k_d (s^{-1})[a]
1	5	90	145	$4x10^{-5}$
2	0.6	91	138	$3x10^{-4}$
SBA_{28}-3	15	100	149	$1x10^{-5}$
SBA_{108}-3	9	100 (82)[b]	147	$2x10^{-5}$
SBA_{227}-3	9	100	147	$2x10^{-5}$
SBA_{28}-3*	15	99	149	$1x10^{-5}$
SBA_{108}-3*	10	100	147	$2x10^{-5}$
SBA_{227}-3*	9	91	147	$2x10^{-5}$
SBA_{52}-4	9	100	147	$2x10^{-5}$
SBA_{78}-4	9	100	147	$2x10^{-5}$
SBA_{283}-4	1	67	139	$2x10^{-4}$
SBA_{56}-5	10	100	148	$2x10^{-5}$
SBA_{92}-6	19	76	149	$1x10^{-5}$
SBA_{92}-6*	9	63	147	$2x10^{-5}$

[a] 130 °C. [b] 160°C.

These results showed that the thermal homolysis of the C-O bond in the pore was as effective as in solution.

In a second time, the incidence of the localization of the alkoxyamine in the mesoporous silica was investigated. For this purpose, two structurally-related bis-alkoxyamines, **5** and **6**, were selected to be located either in the framework (**SBA_{56}-5**) or on the pore surface (**SBA_{92}-6**) of the hybrid material. As previously mentioned, the necessity to have two trialkoxysilane groups on **5**, to position the precursors in the wall, led to the presence of two benzylic alkoxyamines moieties. The homolysis of the first C-O bond leads to a benzylic radical which weakens the second C-O bond and makes its homolysis easier; it is the reason why a direct comparison between **SBA_{56}-5** and **SBA_n-3** was not relevant. This made it necessary to introduce in **SBA_{92}-6** the same benzylic moiety as in **SBA_{56}-5**. After 3 days, the heating of **SBA_{56}-5** in *tert*-butylbenzene at 130 °C led to the quantitative formation of nitroxides whereas **SBA_{92}-6** yielded 76% of radicals after 5 days (Table 1). A close yield of 63% was recorded with the passivated silicas **SBA_{92}-6*** after 2.5 days. Although correct, the pore functionalized silica led to substantially lower yields. This bis-alkoxyamine model showed that the location of the precursor in the silica was not an obstacle to its thermal homolysis. However, longer reaction times were needed to reach the level of cleavage observed for the mono-alkoxyamines. Two reasons might be put forward to explain this difference. In the case of **SBA_{56}-5**, namely when the precursor was embedded in the silica, once the bis-benzylic moiety was removed from the cavity the reverse trapping reaction became unlikely. Its removal, from the cavity via the silica microporosities, should be slow but irreversible. The elimination of the benzylic moiety was ascertained by ^{13}C solid NMR with the disappearance of the aromatic carbon signals. For **SBA_{92}-6**, the situation was different since the first homolysis could release either a carbon-centered radical bearing an alkoxyamine or a TEMPO (Scheme 7). In both case, a radical specie diffused in the silica pore. Once a TEMPO was released, the concentration in free radical trap increased in the medium and became available to react with any carbon-centered radical (Scheme 7A). The second possible cleavage led to

the release of a carbon-centered radical, this transient radical could evolve as for **1** or **SBA$_n$-3**, i.e. dioxygen trapping and dimerization, but it could also be trapped with free TEMPO or underwent a second homolytic cleavage (Scheme 7B). In summary, in both cases, the first homolytic reaction could give rise to subsequent reactions which slowed down the global rate of the overall process.

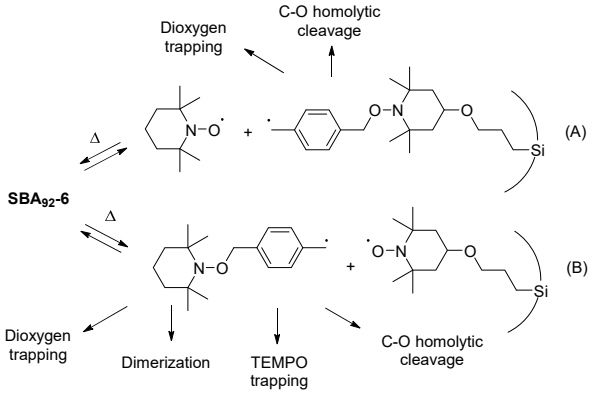

Scheme 7. Homolytic cleavage of **SBA$_{92}$-6**

In order to grasp the effect of the confinement on the alkoxyamine behaviour, the rate constants of the C-O bond cleavage (k_d) and the activation energies (E_a) were measured from CW-experiments in the presence of dioxygen as alkyl radical scavenger, with a classical method (Table 1) [32]. All the values are gathered in Table 1, they were in fair agreement with data reported in previous studies [**Erreur ! Signet non défini.**,32]. The k_d calculated for **SBA$_n$-3** and **SBA$_n$-3*** were about two times lower than for the same alkoxyamine **1** in solution. However, no effect of the passivation could be noticed since the constants were the same for both series of materials. The same trend was observed with **SBA$_{52}$-4** and **SBA$_{78}$-4** for which the dissociation constants were 7 times lower than for the reference **2**. Surprisingly, the behaviour of **SBA$_{283}$-4** was very close to **2** with a k_d almost identical. We did not have an explanation for this reproducible result. The study on these simple alkoxyamines showed that the thermally triggered homolysis can be considered as effective as in solution but needs longer reaction times which could be explained by a more important persistent radical effect (PRE) related to higher radical local concentrations in the pore volume than in solution.

Indeed, whatever the system **SBA_n-3** or **SBA_n-4**, the lowest $t_{1/2}$ values matched with the lowest loadings which released upon cleavage the weakest nitroxide quantity.

3.5 Photochemical homolysis

A 10^{-4}M solution of alkoxyamine **2** was directly irradiated in a 4 mm quartz tube at 360 nm in *tert*-butylbenzene in the EPR cavity. After 15 min, the signal reached a quasi-stationary state which fitted with a yield of 68% (Table 2). In order to control if an irradiation at 100% of the light power could be the source of degradation, the same experiment was performed with a light set at 10 and 20% of the nominal power of the light source. No effect was measured under these conditions since in both cases a 63% yield was recorded after 15 min. For the following studies, 100% of the light power was used.

Table 2. Photochemical homolysis yields and $t_{1/2}$ for **1**, **2**, **SBA_n-4** and **SBA_n-4***

	$t_{1/2}$ (min)	Yield (%)
1	-	0
2	0.3	68,[b] 63,[c] 72[d]
SBA_{52}-4	2 (1)[a]	78 (56)[a]
SBA_{78}-4	5 (2)[a]	90 (70),[a] 81,[f] 80,[g] 100[h]
SBA_{283}-4	4 (3)[a]	94 (76) [a]
SBA_{52}-4*	3	61
SBA_{78}-4*	2	81
SBA_{283}-4*	2	100

[a] without solvent under air, [b] 100% of light power under air, [c] 10 and 20% of light power under air, [d] under argon. [f] in MeOH, [g] in MeOH/AcOH, [h] CH_3CN.

Based on the fragmentation mechanism proposed in the literature (Scheme 2), the nature of the atmosphere should have a direct impact on the fate of the reaction since the formation of TEMPO results from the oxidation of **TEMPO-H** by dioxygen. Thus, the same experiment was performed under an argon atmosphere on a solution degassed with three freeze-pump-thaw cycles with a 10^{-5} mbar vacuum pump. Much to our surprise, no effect was detected, a similar yield of 72% was recorded. This result did not agree with the literature, another mechanism must explain the oxidation of the hydroxylamine. In order to assess the stability of **TEMPO-H** under these experimental

conditions, a 10^{-4} M degassed solution of **TEMPO-H** in *tert*-butylbenzene was irradiated under argon at 360 nm in the EPR cavity (Scheme 8). In the dark, a small residual triplet signal corresponding to TEMPO was observed, then after illumination the intensity of the signal was increased 6-fold (see EPR spectra in supplementary data). The formation of TEMPO upon irradiation of **TEMPO-H** clearly showed that the oxidation occurred thanks to the O-H bond homolytic photo-cleavage probably through a mechanism analogous to the S-H bond homolysis.[33]

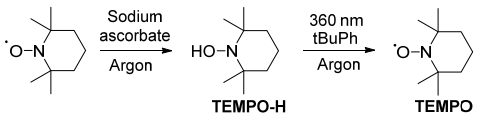

Scheme 8. Photo-oxidation of TEMPO-H

Likewise, suspensions in *tert*-butylbenzene of **SBA$_n$-4** and **SBA$_n$-4*** in EPR quartz tubes were irradiated at 360 nm for 0.5 to 2.5 h. Yields of 78, 90 and 94% were registered for **SBA$_{52}$-4**, **SBA$_{78}$-4** and **SBA$_{283}$-4** (Table 2). Unlike the thermal homolysis, a slight improvement of the yield occurred when the loading decreased. Except for the lower loading, **SBA$_{283}$-4***, the passivation led to a little decrease in the efficacy of the homolysis. In other words, in both cases, the yield increased with the distance between the precursors. The knowledge of the loadings and the surfaces of these materials enabled these distances to be estimated: 2.0, 2.4 and 4.4 nm for **SBA$_{52}$-4**, **SBA$_{78}$-4** and **SBA$_{283}$-4**, respectively. The yield loss might be correlated with the quenching of the excited state of the nitrobenzyl precursor, i.e. the first step of the fragmentation reaction, by a neighbouring TEMPO radicals [34]. Indeed, the closer the nitroxides, the more effective the quenching process and as consequence, the lower the yield.

It can also be underlined that, contrary to the thermal initiation, the passivation increased the fragmentation rate since a plateau was reached in only 30 min. However, it is difficult to compare the passivation incidence on the initiation mode because the mechanisms involved in

the release of the nitroxyl radical are totally different. Nevertheless, as previously mentioned, the substitution of the silanols with trimethylsiloxane groups removed the interaction between the organic precursor and the silica pore surface through hydrogen bonding and, as consequence, favoured its ability to move. This increase in the organic chain mobility was clearly observed by EPR (Figure 4). Indeed, the signal shape of the passivated silica (**SBA_{52}-4***) was closer to the symmetrical triplet of the free TEMPO in solution than the one of **SBA_{52}-4**. This observation was ascertained with the spectrum analysis thanks to the Azz coupling constant which enabled to probe the polarity of organic radical surrounding. Azz values for **SBA_{52}-4** and **SBA_{52}-4***were 33.1 and 31.9 G, respectively. The highest measured constant highlighted the presence of interactions with the local environment of the radical namely the silanol groups whereas after passivation, i.e. a hydrophobic surface, a decrease of the coupling constant was registered.

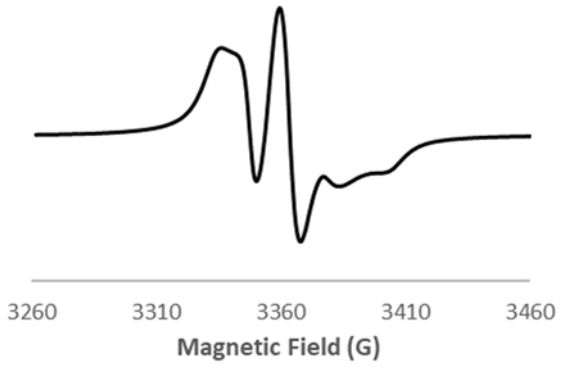

a)

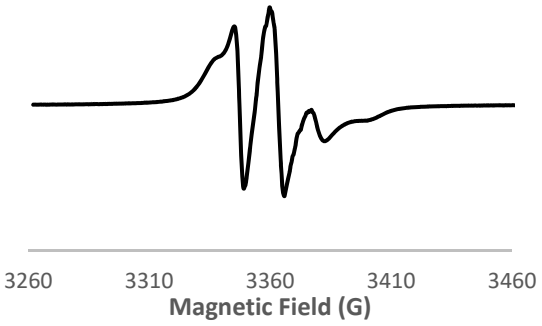

b)

Figure 4. EPR spectra after irradiation of **SBA_{52}-4** (a) and **SBA_{52}-4*** (b)

The effect of polar and/or protic solvents on the formation of nitroxide radical was also investigated. Because of the dielectric constants of these solvents, it was impossible to

perform the study directly in a 4 mm EPR quartz tube. It is the reason why the silicas were irradiated in the solvent of interest then filtered off, washed and dried. These experiments were done in the presence of methanol, methanol/ acetic acid (9/1) and acetonitrile. The EPR analyses of these samples in *tert*-butylbenzene showed a modest yield dispersity. 80, 81 and 100% were measured, respectively (Table 2). As already stated [24,26], the best solvent was acetonitrile for which the yield was quantitative. These values are closed to the 90% value observed in *tert*-butylbenzene.

Finally, **SBA_n-4** silicas were irradiated without solvent, under these conditions the organic chains were refolded onto the surface and displayed a weak mobility as emphasized by the A_{zz} coupling constant value of 35.0 G. A drop of yield of 20% was observed for the three loadings (Table 2). Although noticeable, this decrease showed that, even under unfavourable conditions, the fragmentation was still the main process occurring and as already stated with the experiments in solution the lower yields were registered for the highest loadings.

4. Conclusion

Radical formation occurs efficiently in solution upon thermal or photo-chemical activation. Functionalized mesoporous silicas were designed and prepared to investigate the effectiveness of these activation modes on the generation of radicals of which the precursors were differently located in the material. In order to overcome the difficulty of quantifying the formation of transient radicals, alkoxyamine models were selected as precursors of stable nitroxides. The comparison of different calibration systems clearly showed that to have reliable results they must be structurally as close as possible to the models investigated. Thus, covalently TEMPO pore-functionalized silicas were prepared and used for the quantification of the activation mode efficacy. The heating of alkoxyamine-functionalized silicas led to the formation of the corresponding nitroxyl radicals with yields as good as those registered for the

reaction performed in solution. The main difference lied in the reaction rates which were much slower in the material than in solution. This slowdown could be explained by a higher impact of persistent radical effect due to a higher local radical concentration in the mesoporous silicas. The more the reaction progressed, the more the pore local nitroxide concentration increased, and therfore the probability of trapping benzyl radicals increased which slowed down TEMPO generation. Namely, this effect is related to the radical mechanism formation and not to the thermal activation. Furthermore, this study enabled to determine C-O bond dissociation constants of alkoxyamines covalently linked to a mesoporous silica, which were comparable to those measured in solution. Similarly, the UV irradiation enabled a radical formation comparable to the one observed in solution. This study clearly demonstrates that these two activation modes can be used in mesoporous silicas without a significant loss of efficacy. The low concentration of transient radicals registered in our previous works cannot be explained by the inefficiency of these modes of formation and must be related to other phenomena that are currently under investigation.

Declaration of competing interest

The authors declare that they have no competing financial interest.

Credit authorship contribution statement

Pierre Nabokoff : Investigation, Methodology. **Stéphane Gastaldi :** Conceptualization, Investigation, Methodology, Funding acquisition. **Eric Besson :** Conceptualization, Investigation, Methodology, Funding acquisition.

Acknowledgments

The authors acknowledge the Agence Nationale de la Recherche for funding (ANR-12-JS07-005 and ANR-18-CE29-007). The authors are also grateful to the EPR facilities available at the national EPR network (IR CNRS 3443) and the Aix-Marseille Université EPR center.

Supplementary data: Preparation and characterizations of the organic compounds and the derived materials (NMR, TEM, SAXS, Nitrogen adsorption/desorption analysis, ATG). EPR spectra and growth curves.

References

[1] R.G. Hicks, Org. Biomol. Chem. 5 (2007) 1321–1339. https://doi.org/10.1039/B617142G

[2] B. Tang, J. Zhao, J.-F. Xu, X. Zhang, Chem. Sci. 11 (2020) 1192–1204. https://doi.org/10.1039/C9SC06143F

[3] B. Lü, P. Li, B. Wang, K. Müllen, M. Yin, Nat. Commun. 10 (2019) 767. https://doi.org/10.1038/s41467-019-08434-4

[4] S. Gu, S. Wu, L. Cao, M. Li, N. Qin, J. Zhu, Z. Wang, Y. Li, Z. Li, J. Chen, Z. Lu, J. Am. Chem. Soc. 141 (2019) 9623–9628. https://doi.org/10.1021/jacs.9b03467

[5] C. Dol, G. Gerbaud, B. Guigliarelli, E. Bloch, S. Gastaldi, E. Besson, Phys. Chem. Chem Phys. 21 (2019) 16337−16344. https://doi.org/10.1039/C9CP03052B

[6] C. Dol, F. Vibert, M. P. Bertrand, J. Lalevée, S. Gastaldi, E. Besson, ACS Macro Lett. 6 (2017) 117−120. https://doi.org/10.1021/acsmacrolett.6b00949

[7] B. A. DeHaven, J. T. Tokarski III, A. A. Korous, F. Mentink-Vigier, T. M. Makris, A. M. Brugh, M. D. E. Forbes, J. van Tol, C. R. Bowers, L. S. Shimizu, Chem. Eur. J. 23 (2017) 8315–8319. https://doi.org/10.1002/chem.201701705

[8] T. Hirano, W. Li, L. Abrams, P. J. Krusic, M. F. Ottaviani, N. J. Turro, J. Am. Chem. Soc. 121 (1999) 7170–7171. https://doi.org/10.1021/ja9912628

[9] A. Moscatelli, Z. Liu, X. Lei, J. Dyer, L. Abrams, M. F. Ottaviani, N. J. Turro, J. Am. Chem. Soc. 130 (2008) 11344–11354. https://doi.org/10.1021/ja801487v

[10] S. Fukuzumi, A. Itoh, T. Suenobu, K. Ohkubo, J. Phys. Chem. C 118 (2014) 24188−24196. https://doi.org/10.1021/jp508155u

[11] W. S. Jeon, H.-J. Kim, C. Lee, K. Kim, Chem. Commun. (2002) 1828–1829. https://doi.org/10.1039/B202082C

[12] R. Eelkema, K. Maeda, B Odell, H. L. Anaderson, J. Am. Chem. Soc. 129 (2007) 12384–12385. https://doi.org/10.1021/ja074997i

[13] Q. Song, F. Li, Z. Wang, X. Zhang, Chem. Sci. 6 (2015) 3342–3346. https://doi.org/10.1039/C5SC00862J

[14] X. Zhao, F. Liu, Z. Zhao, H. Karoui, D. Bardelang, O. Ouari, S. Liu, Org. Biomol. Chem. 16 (2018) 3809–3815. https://doi.org/10.1039/C8OB00664D

[15] A. Stergiou, J. Rio, J. H. Griwatz, D. Arčon, H. A. Wegner, C. P. Ewels, N. Tagmatarchis, Angew. Chem. Int. Ed. 58 (2019) 17745–17750. https://doi.org/10.1002/anie.201909126

[16] V. P. Rao, M. B. Zimmt, N. J. Turro, J. Photochem. Photobiol. A: Chem. 60 (1991) 355–360. https://doi.org/10.1016/1010-6030(91)90037-T

[17] G. Pagona, G. Rotas, A. N. Khlobystov, T. W. Chamberlain, K. Porfyrakis, N. Tagmatarchis, J. Am. Chem. Soc. 130 (2008) 6062–6063. https://doi.org/10.1021/ja800760w

[18] F. Simon, H. Kuzmany, J. Bernardi, F. Hauke, A. Hirsch, Carbon 44 (2006) 1958–1962. https://doi.org/10.1016/j.carbon.2006.02.001

[19] F. Vibert, S. R. A. Marque, E. Bloch, S. Queyroy, M. P. Bertrand, S. Gastaldi, E. Besson, Chem. Sci. 5 (2014) 4716–4723. https://doi.org/10.1039/C4SC01907E

[20] F. Vibert, S. R. A. Marque, E. Bloch, S. Queyroy, M. P. Bertrand, S. Gastaldi, E. Besson, J. Phys. Chem. C. 2015, 119, 5434–5439. https://doi.org/10.1021/jp5117382

[21] F. Vibert, E. Bloch, M. P. Bertrand, S. Queyroy, S. Gastaldi, E. Besson, New J. Chem. 41 (2017) 6678–6684. https://doi.org/10.1039/C7NJ00891K

[22] F. Vibert, E. Bloch, M. P. Bertrand, S. Gastaldi, E. Besson, J. Phys. Chem. C. 122 (2018) 681–686. https://doi.org/10.1021/acs.jpcc.7b10879

[23] S. Marque, C. Le Mercier, P. Tordo, H. Fischer, Macromolecules 33 (2000) 4403–4410. https://doi.org/10.1021/ma9918452

[24] I. Seven, T. Weinrich, M. Gränz, C. Grünewald, S. Brüß, I. Krstić, T. F. Prisner, A. Heckel, M. W. Göbel, Eur. J. Org. Chem. (2014) 4037–4043. https://doi.org/10.1002/ejoc.201301692

[25] Y. V. Il'ichev, J. Wirz, J. Phys. Chem. A 104 (2000) 7856–7870. https://doi.org/10.1021/jp000261v

[26] Y. V. Il'ichev, M. A. Schwörer, J. Wirz, J. Am. Chem. Soc. 126 (2004) 4581–4595. https://doi.org/10.1021/ja039071z

[27] A. Baschieri, L. Valgimigli, S. Gabbanini, G. A. DiLabio, E. Romero-Montalvo, R. Amorati, J. Am. Chem. Soc. 140 (2018) 10354−10362. https://doi.org/10.1021/jacs.8b06336

[28] A. Mehdi, C. Reye, R. Corriu, Chem. Soc. Rev. 40 (2011) 563–574. https://doi.org/10.1039/B920516K

[29] J. E. Lofgreen, G. A. Ozin, Chem. Soc. Rev. 43 (2014) 911–933. https://doi.org/10.1039/C3CS60276A

[30] E. Besson, F. Ziarelli, E. Bloch, G. Gerbaud, S. Queyroy, S. Viel, S. Gastaldi, Chem. Commun. 52 (2016) 5531–5533. https://doi.org/10.1039/C6CC01809B

[31] D. Gajan, M. Schwarzwälder, M. P. Conley, W. R. Grüning, A. J. Rossini, A. Zagdoun, M. Lelli, M. Yulikov, G. Jeschke, C. Sauvée, O. Ouari, P. Tordo, L. Veyre, A. Lesage, C. Thieuleux, L. Emsley, C. Copéret, J. Am. Chem. Soc. 2013, 135, 15459–15466. https://doi.org/10.1021/ja405822h

[32] D. Bertin, D. Gigmes, S. R. A. Marque, P. Tordo, Macromolecules 38 (2005) 2638–2650. https://doi.org/10.1021/ma050004u

[33] Y. M. Riyad, R. Hermann, O. Brede, Chem. Phys. Let. 376 (2003) 776–780. https://doi.org/10.1016/S0009-2614(03)01073-X

[34] S. Jockusch, M. Porel, V. Ramamurthy, N. J. Turro, J. Phys. Chem. Lett. 2 (2011) 2877–2880. https://doi.org/10.1021/jz201328f